Available online at www.sciencedirect.com
SCIENCE DIRECT®
International Journal of Pharmaceutics 317 (2006) 175–186
INTERNATIONAL JOURNAL OF PHARMACEUTICS
www.elsevier.com/locate/ijpharm

Characterising the size and shape of polyamidoamines in solution as a function of pH using neutron scattering and pulsed-gradient spin-echo NMR

Zeena Khayat [a,b], Peter C. Griffiths [b,*], Isabelle Grillo [c], Richard K. Heenan [d], Stephen M. King [d], Ruth Duncan [a]

[a] *Centre for Polymer Therapeutics, Welsh School of Pharmacy, King Edward's VII Avenue, Cardiff CF10 3XF, UK*
[b] *School of Chemistry, Cardiff University, Main Building, Park Place, Cardiff CF10 3AT, UK*
[c] *Institut Laue-Langevin, 6 rue Jules Horowitz, BP156-38042 Grenoble, Cedex 9, France*
[d] *ISIS Facility, Rutherford Appleton Laboratory, Chilton, Oxfordshire OX11 0QX, UK*

Received 20 July 2005; received in revised form 5 March 2006; accepted 7 March 2006
Available online 12 March 2006

Abstract

Bioresponsive polymers are being developed as synthetic viral mimetics to enhance the intracellular delivery of macromolecular therapeutic agents such as genes, proteins and peptides. In this context we have designed pH-responsive, amphoteric polyamidoamines (PAAs) which change conformation on passing from a neutral pH (extracellular) to an acidic pH (endosomal and lysosomal) environments. PAAs have already demonstrated cytosolic delivery of genes and non-permeant toxins (e.g. gelonin and ricin A chain). The aim of this study was to use small-angle neutron scattering (SANS) to investigate the most likely shape of the hydrochloride salt form of one particular PAA (ISA23) in solution, under pH conditions that mimic those the polymer would be expected to encounter during endocytic internalisation (pH 7.4–3). It was shown that models based on a Gaussian coil representation of the polymer conformation described the SANS data better over this pH range than models based on a rod-like conformation. The conformation of ISA23 at 37 °C was expanded (radius of gyration ~ 80 Å) at pH ~ 3 but collapsed with an increase in pH (radius of gyration ~ 20 Å at pH 7.4), a conclusion also reached in a *model-free* analysis of the neutron data. Outside this pH range – at the extremes of high and low pH – the polymer coil collapsed and interpretation of the scattering was slightly complicated by the presence of a very weak structure factor indicating that the polymer coils are highly charged. The PAA concentration did not significantly affect the polymer size over the concentration range 10–50 mg/ml. Characterisation of the dynamics of these polymer solutions – diffusion coefficients and viscosity – *ostensibly* suggest a very different conclusion with the polymer expanding as the pH is increased, but this arises due to weak aggregation of the amphoteric polymer coils.

Keywords: Polymer therapeutics; Endosomolytic polymers; Pulsed-gradient spin-echo NMR; Small-angle neutron scattering; Polyamidoamines

1. Introduction

Despite progress in genomics and proteomics research, it has proved much more difficult than originally envisaged to realise effective and practical therapies based on protein-, peptide- and gene-based therapeutics. The principal challenge remains identification of safe and effective delivery systems able to localise these macromolecular therapeutics to the diseased cells or tissues where they are needed, and once there, promote their efficient delivery to the correct intracellular compartment, usually the cytosol (Wagner, 2004). Retroviral and adenoviral vectors are the favoured tools for gene therapy (Edelstein et al., 2004; Ilarduya and DuzgUnes, 2000). Undeniably, they promote highly efficient gene delivery, but they have also several disadvantages, particularly their mixed safety record. The death of an 18-year-old patient in 1999 due to an acute inflammatory reaction after gene therapy (Raper et al., 2003) and the more recent observation that 2 out of 10 children treated with gene therapy to correct severe combined immunodeficiency disease (SCID) developed a type of leukaemia that was clearly

* Corresponding author. Tel.: +44 29 20875858; fax: +44 29 20874030.
E-mail address: griffithspc@cardiff.ac.uk (P.C. Griffiths).

0378-5173/$ – see front matter © 2006 Elsevier B.V. All rights reserved.
doi:10.1016/j.ijpharm.2006.03.003

caused by the viral vector (Hacein-Bey-Abina et al., 2003) led many to question the risk/benefit of this approach (Check, 2003).

It is widely acknowledged that non-viral vectors offer potential advantages in terms of safety and ease of manufacture (Pack et al., 2005). Lipidic-DNA complexes (lipoplexes) and polymer-based DNA complexes (polyplexes) have been tested in clinical trials (Ohana et al., 2004). Their transfection efficiency is often extremely low and the most popular polymeric vectors used are very toxic (Fischer et al., 2003). Those most frequently used include poly cations, e.g. poly-L-lysine (PLL) (Wu and Wu, 1988) and poly(ethylene imine) (PEI) (Boussif et al., 1995), pH-responsive polyanions such as the poly(ethylacrylic acid) (PEAAc), and related polymers (Murthy et al., 1999), and the cationic poly(amidoamine) (PAMAM) dendrimers (Qin et al., 1998).

A large family of PAAs have now been synthesised. Various structures have been designed for different biomedical applications including heparin binding in blood perfusion filters, metal ion complexation, targetable anticancer PAA conjugates and particularly of importance here, as endosomolytic polymers for cytosolic delivery (reviewed in Ferruti et al., 2002). Our research has designed a family of linear poly(amidoamine)s (PAAs) (Duncan et al., 1994; Richardson et al., 1999; Ferruti et al., 2002) where polymer structure has been systematically optimised to give relatively non-toxic polymers (IC_{50} values > 1 mg/ml over 72 h) that are non-haemolytic at pH 7.4, but show pH-dependent breakage of model membranes (Richardson et al., 1999). Moreover, amphoteric structures can be synthesised, e.g. ISA23 (Ferruti et al., 2000), that do not accumulate in liver after intravenous injection, and that target tumours by the enhanced permeability and retention (EPR) effect (Richardson et al., 1999). ISA23 (Scheme 1) is able to deliver genes (Richardson et al., 2001) and promote cytosolic access of the non-permeant toxins ricin A chain and gelonin (Pattrick et al., 2001a). Recent quantitative subcellular fractionation studies showed that PAA is transiently retained in the endosomal compartment (1 h) before transfer to the lysosomal compartment and that isolated vesicles containing PAAs show enhanced membrane permeability (Pattrick et al., 2001b). The counterion of the PAA strongly affects the pH-dependent membrane interaction (Wan et al., 2004). Nevertheless, PAA toxin delivery is still very poorly efficient, requiring many polymer molecules to deliver a single toxin molecule. Hence there is an urgent need to better understand the physico-chemical properties of PAAs and their precise mechanism of membrane destabilisation so that more efficient second generation systems can be designed.

Relatively few studies have explored PAA physico-chemical properties. Early investigations used potentiometric titration, ^{13}C NMR, viscosity measurements and conformational analysis to examine the structure of a number of cationic PAAs, with different alkyl chain between amino groups. In this case they showed that the stiffness and the flexibility depended on various polymer features (Barbucci et al., 1981), such as degree of protonation.

There is much debate as to the mechanism of endosomal permeabilisation of endosomolytic polymers. Behr and colleagues (Boussif et al., 1995) advanced the polymer "proton-sponge effect" as a mechanism to explain PEI action, and others have suggested that this combines with polymer swelling in the acidic endosomal compartment to cause a local osmotic effect that then disrupts the endosomal membrane (Sonawane et al., 2003). Universal applicability of the proton-sponge hypothesis was recently questioned (Funhoff et al., 2004) when a novel polymer with two tertiary amine groups in each monomeric unit [poly(2-methyl-acrylic acid 2-[(2-(dimethylamino)-ethyl)-methyl-amino]-ethyl ester) (so-called pDAMA)] with pK_a values of ~9, and ~5 was found to form polyplexes, but not to mediate endosomal escape. We believe that PAAs require direct membrane interaction to facilitate endosomal escape. It has also been shown that the counterion present is a vital component of this process (Wan et al., 2004). Observations that PAA-block copolymers (Lavignac et al., 2004), and PAA covalent conjugation via a terminal group leads to decreased membrane activity supports this hypothesis.

Of paramount importance here is the dependence of the polymer conformation on the effective charge of the polymer, the latter controlled via the solution pH and ionic strength. Such an understanding of the physico-chemical properties of endosomolytic PAAs is considered essential to allow further systematic structure optimisation. The conformation – or shape – of the polymer may be quantified using SANS.

Small-angle neutron scattering (SANS) is a particularly powerful tool that can bring a new perspective to the solution conformation of polymer therapeutics (as defined by Duncan in 2003), and also help to probe their mechanism of membrane interaction. SANS has however rarely been applied in this field yet it has been widely used to investigate the conformation of polymers in solution, polyelectrolytes (Nishida et al., 2002; Nakamura et al., 2005), copolymers (Pederson, 2002), at interfaces (Griffiths et al., 2004a; King et al., 2002) and in the presence of surfactant micelles (Aswal, 2003; Bergström et al., 2004; Griffiths et al., 2004a) and dendrimers (Ramzi et al., 2000; Hedden and Bauer, 2003).

A nominally identical ISA23 ($M_w = 42{,}700\ g\ mol^{-1}$; $M_w/M_n = 1.7$) to that studied here has been previously examined by viscosity measurements in solutions at 35 °C buffered at pH 8 with a total ionic strength of 0.3 M (Ferruti et al., 2000). For a series of solutions satisfying the condition $[\eta]c = 0.1$, Ferruti et al. analysed their intrinsic viscosity data in terms of the Mark–Houwink model ($[\eta] = kM^{\alpha}$), concluding that amphoteric PAAs (in particular ISA23) possess rather stiff chains since the parameters $k = 9.53 \times 10^{-5}$ dl/g and $\alpha = 0.85$ were somewhat larger than expected for uncharged polymers of a comparable molecular weight. Further, the power law dependence of the radius of gyration on molecular weight had an exponent of 0.74 – $R \propto M^{0.74}$ – typical of an expanded (but random) coil structure. Ferruti's study also considered the viscosity of solutions of ISA23 as a function of pH with the viscosity decreasing from $\eta_{sp}/c = 0.6$ at pH 11 to a local minimum ($\eta_{sp}/c = 3.0$) at pH 5, before increasing once again below pH 3. Accordingly, this predicts a minimum in hydrodynamic volume coinciding with the isoelectric point of the polymer A similar observation was made by Koetz et al. (1993) for the majority (but not all) of a

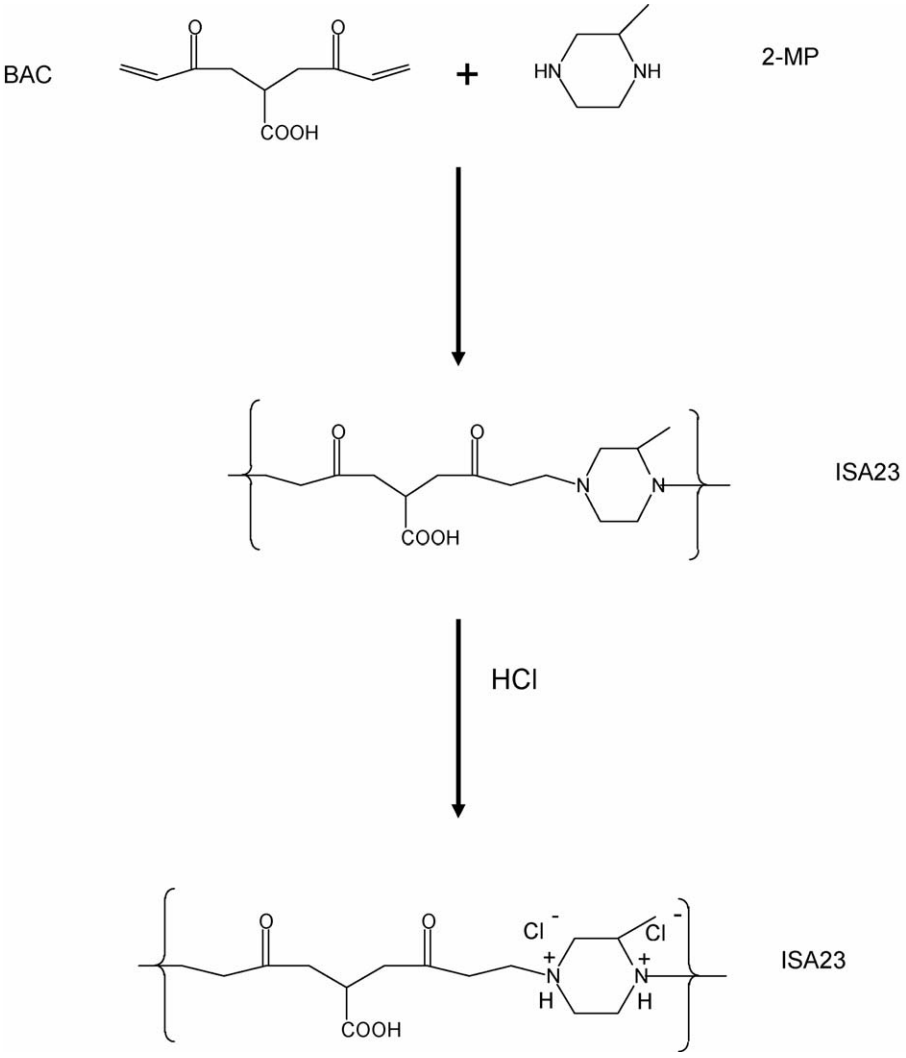

Scheme 1. Synthesis of ISA23.

number of polybetaine-based polyampholytes with differing chemical structure but all containing carboxylic acid groups and various basic nitrogen functions (Koetz et al., 1993). However, Feng and Huang (1997) have shown that polyampholytes of 2-acrylamido-2-methylpropane sulfonic acid (AMPS) and 2-dimethylaminoethyl methacrylate (DMAEMA) exhibit significantly enhanced intrinsic viscosity at the IEP of the polyampholyte.

In contrast to Ferruti's viscosity study, Griffiths et al. in their SANS study on ISA23 found that the PAA polymer coil *expands* as the pH decreases from pH 11 exhibiting a maximum at pH ~ 4—an apparent contradiction to the viscosity data (Griffiths et al., 2004a). The charge versus conformation behaviour of this polymer is rather important as recent experiments suggest that the degree of protonation determines whether an interaction occurs with model surfaces and membranes (surfactant micelles and liposomes). Therefore, the discrepancy between the scattering and viscosity insights needs addressing. The source of the inconsistency could be (i) the "form factor" – the mathematical model that embodies the shape and size of the polymer coil – used in the analysis of the scattering data; (ii) the fact that a structure factor ($S(Q)$) was omitted in the data analysis; or (iii) that the polymer coils are aggregating in solution; the validity of these various approaches is addressed here.

2. Materials and methods

2.1. Materials

The monomer 2,2-bis-(acrylamido)acetic acid (BAC) was synthesised as previously described (Ferruti et al., 1985). Hydrochloric acid (HCl) and sodium hydroxide (NaOH) were purchased from Fisher Scientific UK Ltd. Lithium hydroxide monohydrate ($LiOH{\cdot}H_2O$) and 2-methyl piperazine (2-MP), were purchased from Fluka. 2-MP was recrystallised from *n*-heptane and its purity was determined titrimetrically before use. Phosphate buffered saline tablets (PBS) (Oxoid Ltd., Basingstoke, UK) and deuterated water (D_2O) (Goss Scientific Instruments Ltd.) were used as supplied.

2.2. Synthesis of ISA23

ISA23 was synthesised as previously described (Richardson et al., 1999; Ferruti et al., 2000) by polyaddition of BAC and 2-MePip (Scheme 1). BAC (1 g; 5 mmol) and $LiOH{\cdot}H_2O$ (0.212 g; 5 mmol) were dissolved in double distilled water (1.67 ml, amount required to make 3 M of BAC), this mixture was stirred for 10 min or until all the chemicals have dissolved. To this mixture 2-MP (0.511 g; 5 mmol) was added. The reaction was stirred for 3 days at 25 °C under a nitrogen atmosphere in the dark. After this period, the reaction was stopped by dilution. HCl was then added to the mixture, until the pH reached 3–4. The reaction products were filtered using a stirred ultrafiltration cell (model 8200, Amicon Bioseparation, Millipore), with a membrane cut off of 10,000 g mol^{-1}. The molecular weight distribution of the polymer was then quantified using gel permeation chromatography (GPC) against poly(vinyl pyrrolidone) (PVP) standards.

2.3. Sample preparation

The ISA23 samples were generally prepared by dissolving a known mass of polymer in D_2O containing phosphate buffer (PBS). The pH of the buffered solution drops following the addition of ISA23, and is subsequently adjusted to the desired pH by adding concentrated NaOH or HCl.

2.4. Small-angle neutron scattering

The SANS experiments were conducted on the LOQ diffractometer at the ISIS Spallation Neutron Source (Oxfordshire), and the D11 and D22 diffractometers at the ILL (Grenoble). LOQ is a fixed-geometry, time-of-flight (TOF), instrument whereas D11 and D22 are variable-geometry fixed wavelength instruments. Neutron wavelengths between 2 and 10 Å (LOQ) or 8 Å (D11) or 6 Å (D22) were employed to span Q-ranges (see below) of approximately 0.001–0.6 $Å^{-1}$. In all cases the samples were placed in 2 mm pathlength, UV-spectrophotometer grade, quartz cuvettes (Hellma Ltd., UK) and mounted in aluminium holders on top of an enclosed, computer-controlled, sample changer. The sample volume was approximately 0.4 ml. Temperature control was achieved through the use of a thermostated circulating bath pumping fluid through the base of the sample changer. Under these conditions, a temperature stability of 0.5 °C could be achieved. Experimental measuring times were approximately 40 min per sample.

Dependent on which instrument was used, all scattering data were (a) normalised for the sample transmission and incident wavelength distribution, (b) background corrected using a solvent filled quartz cell (this also removes the inherent instrumental background arising from vacuum windows, etc.), and (c) corrected for the linearity and efficiency of the detector response using the instrument-specific software package. The data were put onto an absolute scale by reference to the scattering from a well-characterised partially deuterated polystyrene-blend standard (LOQ) or a 1 mm thick sample of water (D11, D22).

In a SANS measurement, the neutron beam is scattered by the nuclei of atoms in the sample through an angle (θ). The angle is expressed in terms of a scattering vector, $Q = (4\pi/\lambda)\sin(\theta/2)$, where θ is the scattering angle and λ the neutron wavelength. The scattered intensity, $I(Q)$, from a polymer solution with volume fraction ϕ_p, as a function of this wavevector Q, is given to a good approximation by

$$I(Q) = V_p\varphi_p(\rho_p - \rho_m)^2 P(Q)S(Q) + B_{inc} \quad (1)$$

where V_p is the volume of the particle; $(\rho_p - \rho_m)^2$ the contrast term; $P(Q)$ and $S(Q)$ the form and structure factors, respectively; and B_{inc} is the incoherent background. The form factor $P(Q)$ contains information about the size and shape of the polymer in solution, whilst $S(Q)$ accounts for interactions between the scattering objects. For a dilute solution or non-interacting polymer coils, $S(Q) = 1$ and may be neglected. This assumption was made in the original data analysis. Given the knowledge of the chemical composition of the polymer and its concentration, the pre-factors in Eq. (1) may be estimated. The approach to data analysis is therefore to calculate the theoretical scattering from a model in terms of the parameters describing the size and shape of the polymer. "Best fit" values of these parameters were then determined via an iterative non-linear least squares process. The model is selected based on a priori knowledge, comparison to related systems or commonly, starting from a model-free Guinier analysis. For the latter case, B_{inc} needs to be carefully subtracted; here this was done by fitting a linear relationship to the measured scattering intensity over the last 15 points of the data (i.e. over a Q range where only incoherent scattering is present).

2.5. Pulsed-gradient spin-echo NMR experiments

The self-diffusion coefficients were measured on a Bruker AMX360 NMR spectrometer using a 5 mm diffusion probe (Cryomagnet Systems, Indianapolis), a Bruker gradient spectroscopy accessory and a stimulated echo sequence.

The self-diffusion coefficient D_s is extracted by fitting the integrals for a given peak to the following equation:

$$A(\delta, G, \Delta) = A_0 \exp[-(kD_s)] \quad (2)$$

where $A(\delta,G,\Delta)$ is the signal integral in the presence and A_0 is the absence of the gradients. $k = -\gamma^2G^2([30\Delta(\delta+\sigma)^2 - (10\delta^3 + 30\sigma^2\delta + 14\sigma^2)]/30)$ where γ is the magnetogyric ratio, Δ the diffusion time (0.24 s), σ the gradient ramp time (250 μs), δ the gradient pulse length (400 μs < δ < 2.8 ms) and G the field gradient strength (0.86 T m^{-1}) i.e. typically 3.8 A into a coil with $dG/dI = 0.227$ T m^{-1} A^{-1}.

3. Results and discussion

Consider the absolute intensity of the scattering, Fig. 1(a). For the data recorded at the ILL and for the particularly weak scattering systems, there is an upturn in scattering at low Q. This may be due to aggregation – an attractive interaction – although in our earlier treatment of related data, this was considered to be an artefact since (i) no such scattering was observed in similar samples recorded at ISIS and (ii) the Q dependence of this upturn is unphysical (i.e. greater than Q^{-4}). Accordingly initially at least,

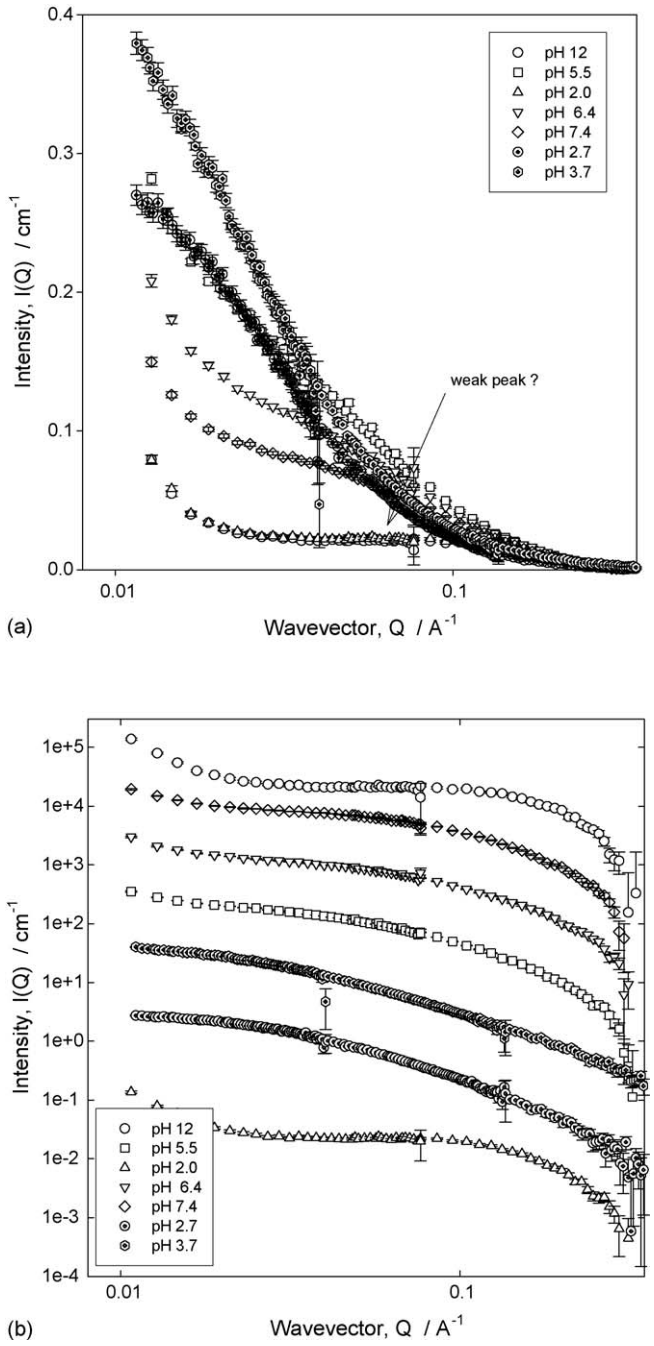

Fig. 1. (a) Small-angle neutron scattering for ISA23 (5 wt.%) in D_2O as a function of pH; (b) small-angle neutron scattering for ISA23 (5 wt.%) in D_2O as a function of pH. Each dataset has been offset by a factor of 10.

ignore the first two or three datapoints in the following analysis. As Q tends to zero, the factors $P(Q)$ and $S(Q)$ in Eq. (1) also tend to unity, and thus one may write $I(Q \to 0) = V_p \varphi_p (\rho_p - \rho_m)^2$ for a dilute system. From the composition of the polymer, the absolute intensity of the scattering of these solutions and noting that concentration is 50 mg ml^{-1} in D_2O, the volume of the polymer coil (V_p) may be estimated; expressed in terms of a (spherical) radius this corresponds to $R \sim 50$ Å. Equally as important is the simple insight this approach provides into the change in volume due to the effects of pH—clearly, the data with pH 2.0 and 12.0 have least scattering (ignoring the weak upturn in the data) and are therefore, of smallest volume (collapsed). The scattering intensity for the solution at pH 3.7 is most intense, and therefore the polymer coil most expanded.

Overall, the intensity of the various datasets follow the pH order $3.7 > 5.5 \approx 2.7 > 6.4 > 7.4 > 12.0 \approx 2.0$. This apparently random order actually correlates well with a maximum in the volume of the polymer coil extracted from our previous analysis of such data, centred around pH 4.0 (±0.5). The intensities over this pH range change by a factor of 5, corresponding to a change in the effective radius of a factor of ∼2. The data at pH 12.0 and 2.0 are different to those at the other pHs, with a very weak signature of a structure peak around $Q \sim 0.06$ Å. The data have been replotted in Fig. 1(b) with each dataset offset by a factor of 10 in an attempt to emphasis this feature. Such a peak arises due to a highly charged, collapsed structure such as a micelle, unfortunately rendering data interpretation less facile. However, since these polymers will not experience such extreme pHs during internalisation into cells, a rigorous analysis is not warranted.

When the shape of the scattering object is not known, is irregular or not describable in a simple manner, the low Q data from a SANS experiment may be analysed in a model-free fashion to yield an estimate of the size of the scatterer (Guinier and Fournet, 1955). The form factor, $P(Q)$, provided the system is dilute (non-interacting scatterers, $S(Q) = 1$), may be approximated at small Q as

$$P(Q \to 0) = \exp\left(-\frac{Q^2 R_g^2}{3}\right) \tag{3}$$

where R_g is the rms radius of gyration averaged over the volume of the polymer. A Guinier plot ($\ln I(Q)$ versus Q^2) will exhibit a linear portion over the region $QR_g < 1$.

However, to estimate the most likely overall shape of a scatterer, Eq. (3) may be generalised:

$$P(Q) = Q^{-D} \exp\left(\frac{-Q^2 R^2}{K}\right) \tag{4}$$

where R is the characteristic dimension—for a sphere, R corresponds to the radius, $D = 0$ and $K = 5$; for a long thin rigid cylinder, R is the cross-sectional radius, $D = 1$ and $K = 4$ and whilst for large rigid discs, R gives the thickness, $D = 2$ and $K = 12$. Thus, an appropriate form of Eq. (4) $\ln[I(Q)Q^D]$ versus Q^2 will display a linear region in an appropriate Q range if the scatterer conforms to that particular gross morphology, from which the characteristic dimension may be extracted.

To estimate the conformation of ISA23 under different environmental conditions, or to provide a coarse picture of the size at different pH values, the raw data obtained by SANS for ISA23 (37 °C at 50 mg/ml) were analysed in terms of a model-free Guinier analysis. Selected data are presented in Fig. 2(a)–(c) over the Q range for which the Guinier representation is valid ($QR_g < 1$). Clearly, the functional form of Fig. 2(a) exhibits the region of largest linearity, implying that the polymer has a more spherical shape, and one that does not change with pH. Derived radii are discussed later in this paper (Figs. 5 and 7).

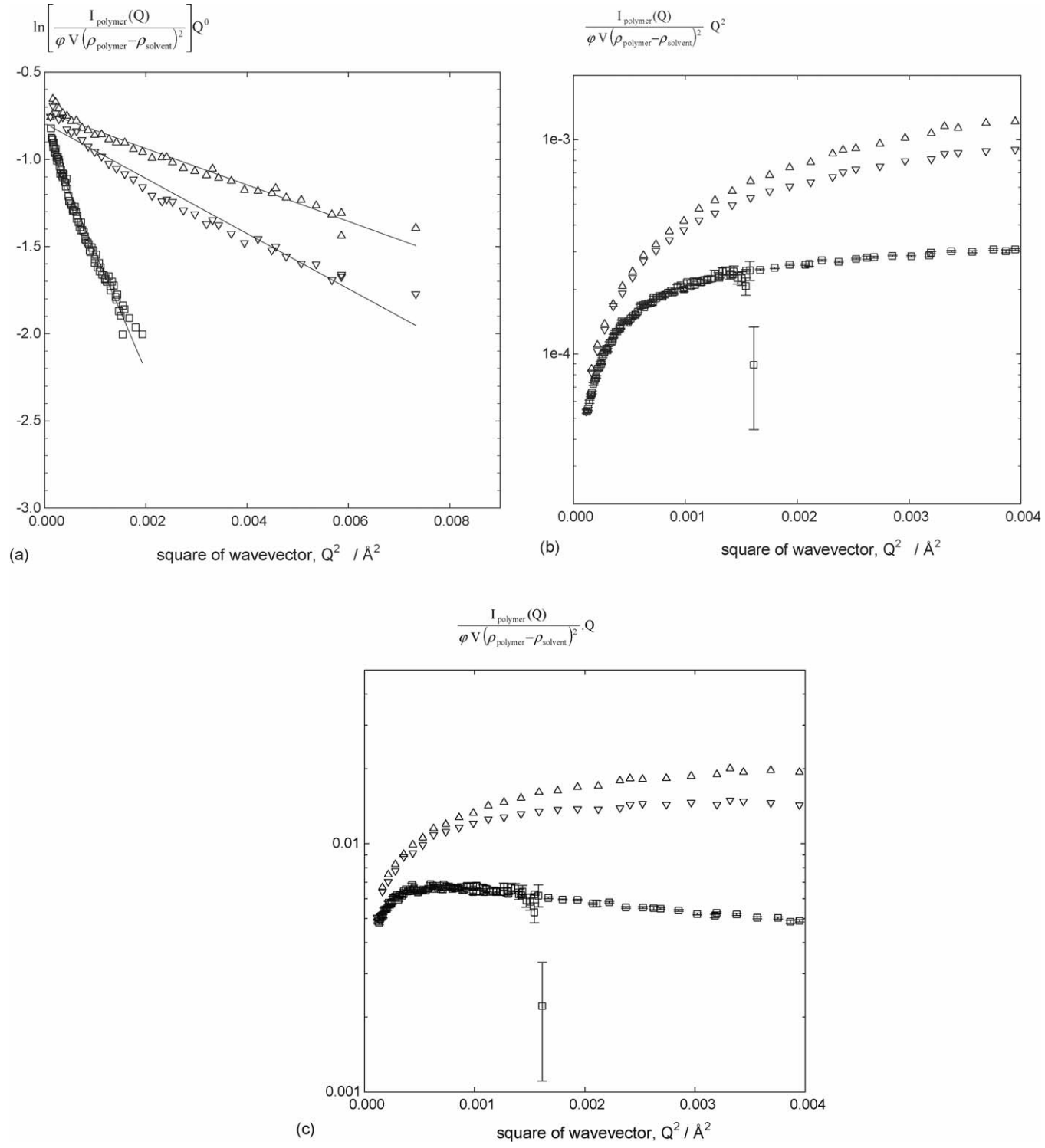

Fig. 2. (a) Spheres Guinier analysis $\ln[I_{\text{polymer}}(Q)/\varphi V(\rho_{\text{polymer}} - \rho_{\text{solvent}})^2]Q^0$ for ISA23 (5 wt.%) D_2O as a function of pH: (□) pH 3.7; (▽) pH 5.5 and (△) pH 7.4. (b) Disk Guinier analysis for ISA23 (5 wt.%) polymer in D_2O as a function of pH: (□) pH 3.7; (▽) pH 5.5 and (△) pH 7.4. (c) Cylinder Guinier analysis for ISA23 (5 wt.%) polymer in D_2O as a function of pH; (□) pH 3.7; (▽) pH 5.5 and (△) pH 7.4.

Whilst such a model-free approach is helpful, a complete analysis of the data requires a somewhat more involved approach in order to fully characterise the polymer conformation. Criteria to assess the most likely shape include not only an appropriate fit to the data but also an assessment of the absolute scattering intensity. Given that upon protonation the polymer becomes charged, and remembering the conclusions drawn from the viscosity data of Ferruti et al. (2000), an appropriate model to test is one that embodies an elongated or "rod-like" morphology.

For semi-flexible polymers in solution, the form factor can be "dissected" into three key parts, defined by an appropriate Q range: (i) at low Q – corresponding to large distances – the

Table 1
Gaussian coil fits to the SANS data—the effect of concentration on the size of ISA23, at pH 7.4 and 5.5

pH	Concentration (mg/ml)	Radius of gyration, R_g (Å)
7.4	10	24.7 ± 1.1
	25	23.5 ± 3.6
	50	21.4 ± 1.1
5.5	10	40.0 ± 2.3
	25	38.5 ± 8.6
	50	32.8 ± 1.1

scattering is sensitive to the overall size of the polymer, and the overall radius of gyration may be determined as outlined in Fig. 2(a)–(c); (ii) over an intermediate Q range, excluded volume effects dominate the conformation of the chain and the classical worm-like chain described by a Kratky–Porod relationship is observed, from which the length of the coil may be calculated; whilst (iii) at high Q, the cross-sectional area of the chain may be extracted (although this is often too small to be seen clearly).

For region (i), a Gaussian coil model may be used (derived by Debye, 1947), modified to include polydispersity:

$$P(Q) = \frac{2[(1+uv)^{-1/v} + u - 1]}{(1+v)u^2} \tag{5}$$

where v is a measure of the polydispersity, $(M_w/M_n) - 1$ and $u = Q^2R_g^2/(1+2v)$ where R_g is the polymer radius of gyration, Fig. 3(a). As may be seen, the Gaussian coil model does provides good fits to the data (the extremes of pH have been omitted), that are only slightly improved in the presence of a degree of polydispersity comparable to that observed by GPC.

Table 1 presents the fitted radii of gyration for a series of solutions of ISA23 as a function of polymer concentration. Whilst the data form such solutions are rather noisy due to the weak contrast ($(\rho_p - \rho_m)^2$) as in Eq. (1), it is clear that there is no significant change on polymer conformation over a wide range of polymer concentration.

For region (iii), and over the range $2\pi/L < Q < 2\pi/R_c$ where L is the persistence length of the rod:

$$P(Q) \approx \frac{\pi M_L}{Q} \exp\left(-\frac{Q^2R_c^2}{2}\right) \tag{6}$$

M_L denotes the mass per unit length and R_c is the cross-sectional radius of the chain, Fig. 3(b). An unequivocal observation of this dependence requires that the persistence length is reasonably long. A further insight is to compare the functional form of Eq. (6) and that of Eqs. (3) and (5); all three functional forms scale as Q^{-2}.

Finally, for region (iii), the form factor may be considered as that of an infinitely thin needle of length L:

$$P(Q) = \frac{2}{QL}\left(\int_0^{QL} \frac{\sin(QL)}{QL}\,\mathrm{d}(QL) - \frac{1-\cos(QL)}{QL}\right) \tag{7}$$

which, at high Q, leads to the scaling Q^{-1} prediction of Eq. (6), $P(Q) \approx \pi/QL$. The prediction that $P(Q) \approx \pi/QL$ should be easily identifiable in the scattering. Fig. 3(c) shows that over the pH QL range studied, such a scaling law does adequately account for the data, including those at the limits of the pH range.

However, whilst considering these limiting behaviours, any appropriate model of the polymer should fit the scattering data over the entire Q range. It should be stated that attempts to fit the data to a model describing the polymer as an infinitesimally thin rod – that would account for a Q^{-1} dependence – were (not unsurprisingly) unsuccessful indicating that the polymer has an appreciable cross-section. The most appropriate model therefore, appears to be one that would incorporate *both* a Gaussian *and* a rod-like or elongated characteristic into the overall polymer conformation. However, this is not unexpected; a polymer coil following Gaussian statistics will inherently demonstrate a rod-like structure over an appropriately short length-scale.

It is appropriate to test these data against two further models; a gel-type model and one that captures both the polyelectrolyte and Gaussian coil limiting behaviour. For the former case – the "polyelectrolyte gel model" – the $P(Q)$ of the polymer is approximately modelled as rod of length L with cross-section R_{ax}:

$$P(Q) \cong \frac{1}{QL}\exp\left(-\frac{Q^2R_{ax}^2}{2}\right)\left(-\frac{Q^2\xi^2}{1+Q^2\xi^2}\right) \tag{8}$$

where the second term accounts for the gel-type structure associated with a correlation length or mesh size ξ. The latter model – the Kholodenko–Dirac worm (Kholodenko, 1993a,b; Hickl et al., 1997) – describes the polymer as a rod-like structure with a radial Guinier characteristic:

$$I(Q) = P_{worm}(Q)P_{axial}(Q) \tag{9}$$

The Kholodenko–Dirac model smoothly interpolates between the Gaussian coil and rigid rod predictions depending on the persistence length l of the polymer. The composite form factors are given by

$$P_{worm}(Q) = \frac{2}{3n}\int_0^{3n}\left(1 - \frac{y}{3n}\right) f(y)\,\mathrm{d}y \tag{10}$$

$$\text{For } Q \le \frac{3}{l},\quad f(y) = \frac{\sinh(Ey)}{E\sinh(y)} \text{ and } E = \left[1 - \left(\frac{Ql}{3}\right)^2\right]^{1/2},$$

$$\text{for } Q > \frac{3}{l},\quad f(y) = \frac{\sinh(Fy)}{F\sinh(y)} \text{ and}$$

$$F = \left[\left(\frac{Ql}{3}\right)^2 - 1\right]^{1/2}$$

The radial cross-section of the worm is the same as the latter part of Eq. (6):

$$P_{axial}(Q) = N(\rho_p - \rho_m)^2(AL)^2\exp(-\tfrac{1}{2}Q^2R_{ax}^2) \tag{11}$$

where A is the cross-sectional area of the polymer worm $A = 2\pi R_{ax}^2$ and L is the contour length, $L = nl$. Again note the similarity of the functional form of Eqs. (3), (6) and (11).

Taking the first of these two models (Eq. (8)), introducing a finite cross-section to the rod yields a better "fit" to the data compared with an infinitely thin model. A typical, illustrative

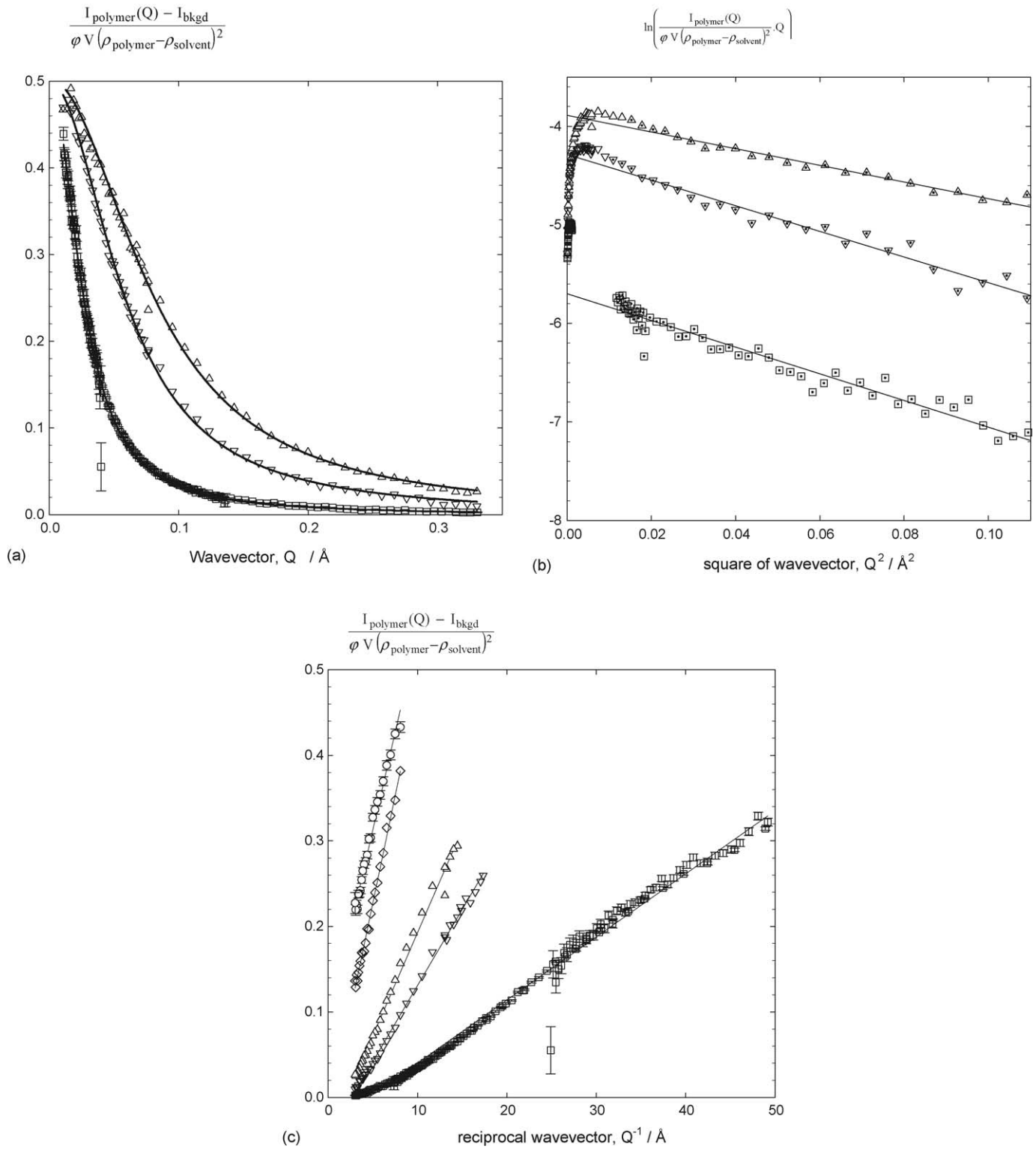

Fig. 3. (a) Normalised SANS data $I_{polymer}(Q) - I_{bkgd}/\varphi V(\rho_{polymer} - \rho_{solvent})^2$ for ISA23 (5 wt.%) polymer in D_2O as a function of pH: (□) pH 3.7; (▽) pH 5.5 and (△) pH 7.4. (b) Cross-sectional analysis for ISA23 (5 wt.%) polymer in D_2O as a function of pH: (□) pH 3.7; (▽) pH 5.5 and (△) pH 7.4. (c) Normalised SANS data $I_{polymer}(Q) - B_{inc}/\varphi V(\rho_{polymer} - \rho_{solvent})^2$ plotted as a function of reciprocal Q (Q^{-1}) for ISA23 (5 wt.%) polymer in D_2O as a function of pH: (◊) pH 2.0; (□) pH 3.7; (▽) pH 5.5; (△) pH 7.4; (◯) pH 13.0.

dataset is presented in Fig. 4(a). The fit is best (but not good) when the cross-sectional radius is 21 Å, with (too) a short length (11 Å) i.e. more spherical than rod-like in shape. ξ is typically slightly longer than L for all cases. For the other pH data, the fits were equally poor, suggesting that the dominant conformation of ISA23 in solution is not rod-like. The approach does invoke a rather distinct interface between the radial structure and the solvent, and in reality this interface will be rather more diffuse,

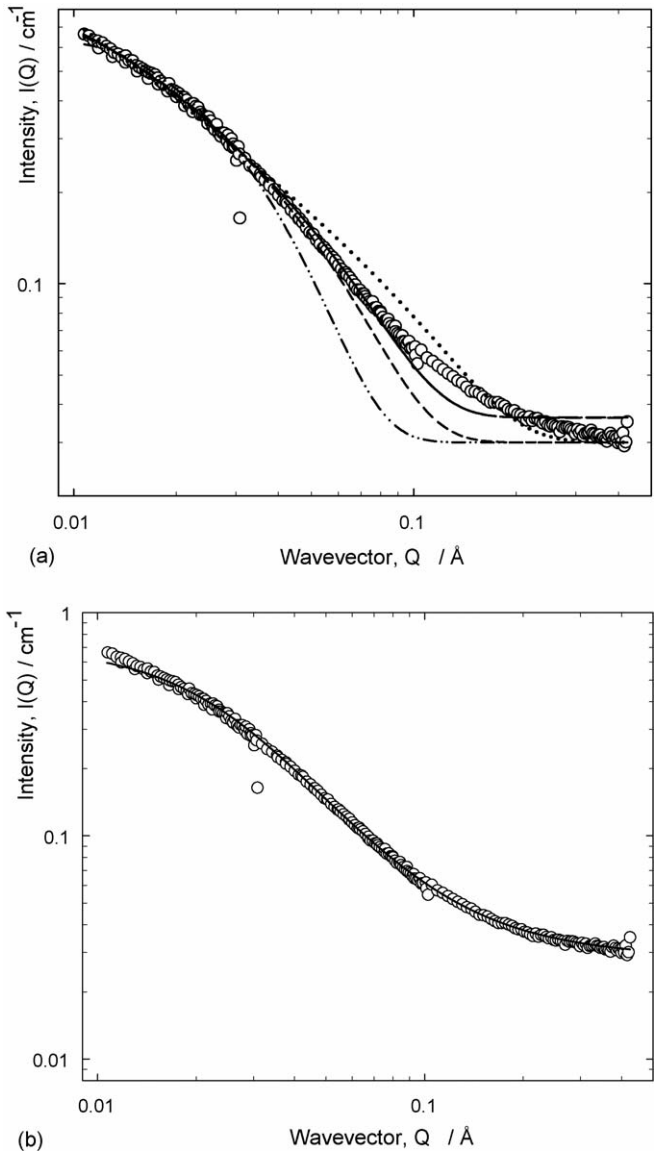

Fig. 4. (a) Small-angle neutron scattering data for ISA23 (5 wt.%) in D_2O at pH 4. The lines represent the fits to the polyelectrolyte model (Eq. (8)) with (i) an unconstrained fit yielding $R_{ax} = 21$ Å, $L = 11$ Å; (ii) fits in which the radius is constrained; $R_{ax} = 10$ Å (dotted line), $R_{ax} = 20$ Å (long dashed black line), $R_{ax} = 30$ Å (dash dotted black line), and (iii) fits in which the length is constrained; $L = 100$ Å (long dashed black line) and $L = 500$ Å (medium dashed black line). (b) Small-angle neutron scattering data for ISA23 (5 wt.%) in D_2O, pH 4.0. The line represents the fits to the Kholodenko–Dirac wormlike chain model (Eqs. (9)–(11)) with $R = 2.2$ Å, $l = 12$ Å, $n = 125$.

which coupled to the polydispersity of the polymer, will render the fit less precise at high Q.

The second model – the Kholodenko–Dirac worm – (Eqs. (9) and (10)) represents a better treatment of the data, Fig. 4(b), and is as good as the Gaussian treatment (Eq. (5)) although it must be stressed that for a flexible chain, the Gaussian and Kholodenko–Dirac worm formulations (Eq. (9)) are equivalent.

Fig. 5 summarises the characteristic parameters extracted from the various analyses of the SANS data. Clearly, these all suggest that the polymer expands as the pH is reduced, reaching a maximum around pH 4.

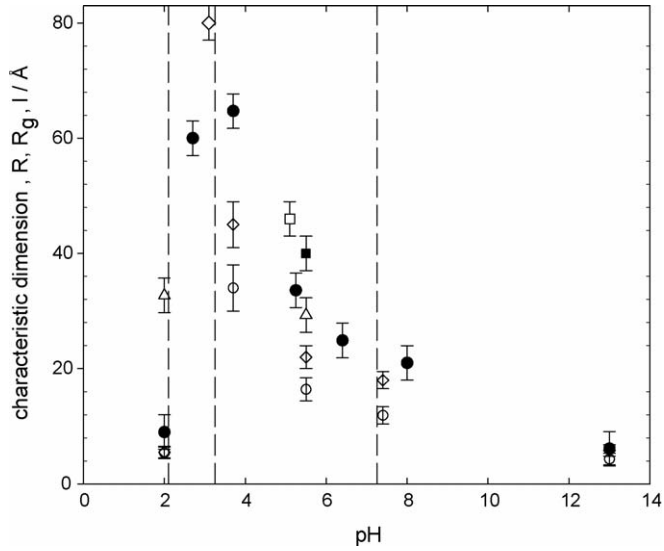

Fig. 5. Characteristic dimension extracted from the various fits to the SANS data: (◊) radius of gyration from a simple spherical Guinier analysis; (Δ, ●) radius of gyration from the Gaussian coil analysis (different counterion polymers) and (◯) correlation length extracted from the Kholodenko–Dirac worm-like chain.

Previous studies, using light scattering and GPC, have shown that ISA23 tends to form aggregates (Mendichi et al., 2005a,b; Ferruti et al., 2000). This could be the source of the discrepancy between the SANS and viscosity data as relatively few aggregates would be required to affect the dynamics of the system (viscosity), but would have little effect on the scattering. Indeed, any scattering from such aggregates would lie beyond the lower boundary of the Q range accessible in these experiments. The ILL data do extend to slightly lower Q values than the ISIS data and a weak upturn is indeed observed but this was discounted as an artefact as discussed previously—accordingly, no definitive statement may be made regarding the presence of any aggregated form of ISA23 from the SANS data.

To explore this facet of the system, we undertook an NMR analysis of the self-diffusion coefficient of ISA23 as a function of pH. A parallel series measurements in which the pH was varied was also studied at a higher ionic strength to probe separately the effects of pH and ionic strength. The presence of a small degree of aggregation would lead to significant changes in diffusion coefficient. Three representative datasets – "attenuation plots" – are presented in Fig. 6 that span the pH range studied. Clearly, the sample at pH 4.5 decays most rapidly and therefore has the largest diffusion coefficient. For polymers that are identical in size (monodisperse) and/or where there is an association or aggregation process occurring on a timescale that is rapid compared with the timescale of the measurements (240 ms), a single exponential relationship should be observed (Eq. (2)) whose slope corresponds to the self-diffusion coefficient. Polydispersity gives rise to upward curvature in the attenuation plot, the degree of which increases with increasing polydispersity. Aggregation that is irreversible (or "slow" on the timescale of the experiment) would give rise to two characteristic slopes – the first corresponding to the diffusion of the aggregates, the sec-

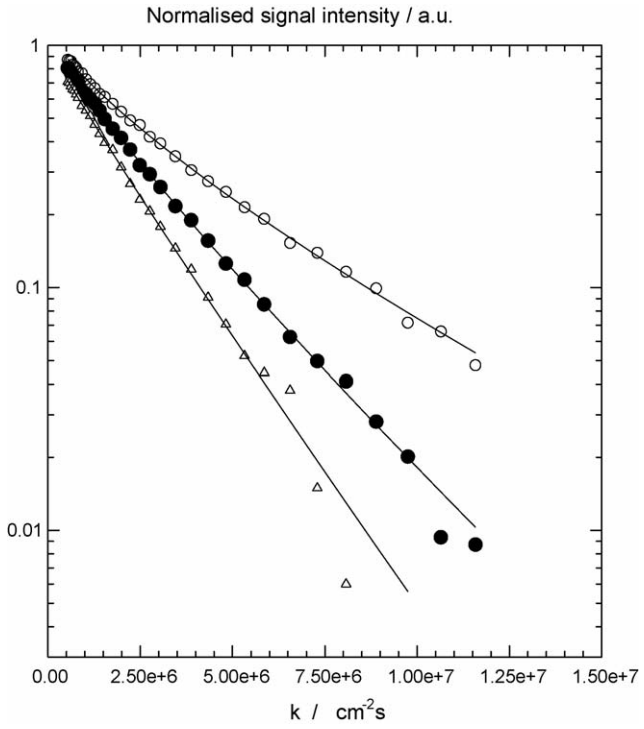

Fig. 6. Typical PGSE-NMR dataset for ISA23 (5 wt.%) in D_2O at 25 °C; pH 4.5 (△), pH 4 (◯) and pH 9 (●). The solid lines correspond to fits to a stretched exponential model that empirically accounts for small degrees of polydispersity.

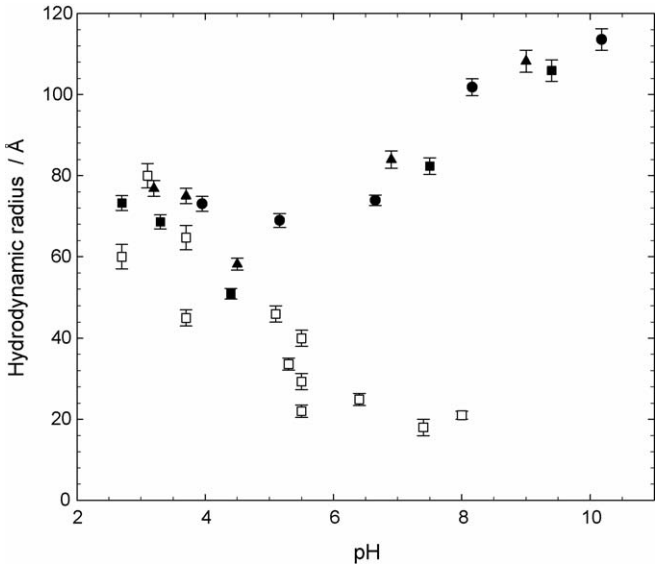

Fig. 7. Hydrodynamic radii superimposed on the "scattering dimension" (□) (Fig. 5) as a function of pH calculated from the self-diffusion coefficients via the Stokes–Einstein equation; (●) 1 wt.% ISA23 in D_2O at 25 °C; (■) 1.5 wt.% ISA23 in 50 mM NaCl/D_2O at 37 °C and (▲) 1.5 wt.% ISA23·HCl in D_2O at 37 °C.

ond the non-aggregated polymers – with the balance of each term being determined by concentration of the polymers in each environment. The only-slight departure from linearity indicates that the polymers are polydisperse but no significantly so, and that no irreversible aggregation is occurring. As might be expected, the effects of polydispersity are manifest more strongly when the polymer is expanded.

Fig. 7 shows the radii of hydration as a function of pH extracted from these NMR diffusion coefficients as a function of pH and the data are superimposed on the SANS results. As found in the viscosity data, the size clearly *decreases* with a decrease in pH attaining a minimum value around pH 43.5 i.e. close to the isoelectric point, before subsequently expanding at pH below 4.5. Interestingly, the agreement between the three approaches is reasonable for pH < 5. There appears to be no significant dependence on temperature or ionic strength.

Equally clear however, is the fact that the NMR and viscosity data display the opposite pH trend with respect to the SANS. Such a disagreement could occur if (i) the polymers are indeed adopting a more elongated structure such that the effective hydrodynamic radius scales as $R^2 = R_{ax}^2 + L^2$ but this would require L to be substantial; this is not observed in the SANS, or (ii) the polymers are indeed aggregating, but the effect would have to be small so as not to contribute significantly to the scattering. The self-association of ISA23 has been detected by SEC for a series of ISA23-based polymers, there being a small fraction of high molecular weight polymer present (Mendichi et al., 2005a,b). Such a component would be largely invisible in the SANS experiment, and provided it was dynamic, could lead to significant discrepancies between the two techniques.

Interestingly pH ≈ 5.6–6.0 coincides with the switch from an overall positively charged polymer at low pH to a net negatively charged polymer above pH 5. Coincidentally, for pH > 5, the ability of these polymer to break the membrane of red blood cells – the degree of haemolysis – is minimal, indicating that either this aggregation reduces the ability of the polymers to interact with the membrane surface or the mechanism that drives aggregation is also involved in the membrane interaction (Griffiths et al., 2004b).

4. Conclusions

When interpreting neutron scattering data it is essential to choose an appropriate mathematical model to allow accurate estimation of the shape and size of the polymer coil in solution. This is not always as easy task as many models predict a particular Q dependence that may or may not be unequivocally demonstrated in the scattering depending in the size of the scatterer. The results presented here amply demonstrate this fact—a Gaussian coil model gives the best fit for ISA23 in solution (except at the limits of pH) but the "signature" of a rigid rod is also seen in the data due to a combination of the local flexibility of the polymer, its over size and the Q range. The Kholodenko–Dirac model captures both these facets and is also shown to provide an accurate treatment of the date. On balance, the polymers exhibit a Gaussian coil conformation – rather than a rod-like conformation – over a wide pH range and polymer concentrations examined (10–50 mg/ml). Irrespective of the precise model adopted however, these results support the proposed mode of action of PAAs; a pH driven coil expansion/rearrangement.

Acknowledgements

ZK would like to thank Cardiff University for supporting her PhD studentship, CCLRC and ILL are thanked for provision of SANS beam time.

References

Aswal, V.K., 2003. Salt effect in ionic mixed micelles. Chem. Phys. Lett. 371, 371–377.

Barbucci, R., Casolar, M., Ferruti, P., Barone, V., Lelj, F.L., Oliva, L., 1981. Macroinorganics. 7. Property–structure relationships for polymeric bases whose monomeric units behave independently toward protonation. Macromolecules 14, 1203–1209.

Bergström, M.L.L., Kjellin, M.U.R., Claesson, P.M., 2004. Small-angle neutron scattering study of mixtures of cationic polyelectrolyte and anionic surfactant: effect of polyelectrolyte charge density. J. Phys. Chem. B 108, 1874–1881.

Boussif, O., Lezoualch, F., Zanta, M.A., Mergnym, M.D., Scherman, D., Demeneix, B., Behr, J.-P., 1995. A versatile vector for gene and oligonucleotide transfer into cells in culture and in vivo: polyethylenimine. Proc. Natl. Acad. Sci. U.S.A. 92, 7297–7301.

Check, E., 2003. Harmful potential of viral vectors fuels doubts over gene therapy. Nature 423, 573–574.

Debye, P., 1947. Molecular-weight determination by light scattering. J. Phys. Colloid Chem. 51, 18–32.

Duncan, R., Ferruti, P., Sgouras, D., Tuboku-Metzger, A., Ranucci, E., Bignotti, F.A., 1994. Polymer–triton X-100 conjugate capable of pH-dependent red blood cell lysis: a model system illustrating the possibility of drug delivery within acidic intracellular compartments. J. Drug Target. 2, 341–347.

Duncan, R., 2003. The dawning era of polymer therapeutics. Nat. Rev. Drug Discov. 2, 347–360.

Edelstein, M.L., Abedi, M.R., Wixon, J., Edelstein, R.M., 2004. J. Gene Med. 6, 560–597.

Feng, J., Huang, R., 1997. Studies on the aqueous solution properties of AMPS-DMAEMA polyampholytes. Gaofenzi Cailiao Kexue Yu Gongcheng 13, 109–113.

Ferruti, P., Marchisio, M.A., Barbucci, R., 1985. Synthesis, physico-chemical properties and biomedical applications of poly(amido-amine)s. Polymer 26, 1336–1348.

Ferruti, P., Manzoni, S., Richardson, S.C.W., Duncan, R., Pattrick, N.G., Mendichi, R., Casolaro, M., 2000. Amphoteric linear poly(amidoamine)s as endosomolytic polymers: correlation between physicochemical and biological properties. Macromolecules 33, 7793–7800.

Ferruti, P., Marchisio, M.A., Duncan, R., 2002. Poly(amido-amine)s: biomedical applications. Macromol. Rapid Commun. 23, 332–355.

Fischer, D., Li, Y.X., Ahlemeyer, B., Krieglstein, J., Kissel, T., 2003. In vitro cytotoxicity testing of poly cations: influence of polymer structure on cell viability and hemolysis. Biomaterials 24, 1121–1131.

Funhoff, A.M., van Nostrum, C.F., Koning, G.A., Schuurmans-Nieuwenbroek, N.M.E., Crommelin, D.J.A., Hennink, W.E., 2004. Endosomal escape of polymeric gene delivery complexes is not always enhanced by polymers buffering at low pH. Biomacromolecules 5, 32–39.

Griffiths, P.C., Paul, A., Khayat, Z., Wan, K.W., King, S.M., Grillo, I., Schweins, R., Ferruti, P., Franchini, J., Duncan, R., 2004a. Understanding the mechanism of action of poly(amidoamine)s as endosomolytic polymers: correlation of physicochemical and biological properties. Biomacromolecules 5, 1422–1427.

Griffiths, P.C., Paul, A., Heenan, R.K., Penfold, J., Ranganathan, R., Bales, B.L., 2004b. Role of counterion concentration in determining micelle aggregation: evaluation of the combination of constraints from small-angle neutron scattering, electron paramagnetic resonance, and time-resolved fluorescence quenching. J. Phys. Chem. B 108, 3810–3816.

Guinier, A., Fournet, G., 1955. Small Angle Scattering of X-rays. Wiley, New York.

Hacein-Bey-Abina, S., von Kalle, C., Schmidt, M., Le Deist, F., Wulffraat, N., Mcintyre, E., Radford, I., Villeval, J.L., Fraser, C.C., Cavazzana-Calvo, M., Fischer, A., 2003. A serious adverse event after successful gene therapy for X-linked severe combined immunodeficiency. New Engl. J. Med. 348, 255–256.

Hedden, R.C., Bauer, B.J., 2003. Structure and dimensions of PAMAM/PEG dendrimer-star polymers. Macromolecules 36, 1829–1835.

Hickl, P., Ballauff, M., Scherf, U., Muellen, K., Lindner, P., 1997. Characterization of a ladder polymer by small-angle X-ray and neutron scattering. Macromolecules 30, 273–279.

Ilarduya, C.T.D., DuzgUnes, N., 2000. Efficient gene transfer by transferrin lipoplexes in the presence of serum. Biochim. Biophys. Acta 1463, 333–342.

Kholodenko, A.L., 1993a. Analytical calculation of the scattering function for polymers of arbitrary flexibility using the Dirac propagator. Macromolecules 26, 4179–4183.

Kholodenko, A.L., 1993b. Scattering function for semiflexible polymers: Dirac versus Kratky-Porod. Phys. Lett. A 178, 1–2.

King, S., Griffiths, P.C., Hone, J., Cosgrove, T., 2002. SANS from adsorbed polymer layers. Macromol. Symp. 190, 33–42.

Koetz, J., Hahn, M., Philipp, B., Bekturov, E.A., Kudaibergenov, S.E., 1993. Inter- and intramolecular interactions in polyelectrolyte complex formation with polyampholytes. Makromol. Chem. 194, 397–410.

Lavignac, N., Lazenby, M., Foka, P., Malgesini, B., Verpilio, I., Ferruti, P., Duncan, R., 2004. Synthesis and endosomolytic properties of poly(amidoamine) block copolymers. Macromol. Biosci. 20, 922–929.

Mendichi, R., Ferruti, P., Malgesini, B., 2005a. Evidence of aggregation in dilute solution of amphoteric poly(amido-amine)s by size exclusion chromatography. Biomed. Chromatogr. 19, 96–201.

Mendichi, R., Ferruit, P., Malgesini, B., 2005b. Evidence of aggregation in dilute solution of amphoteric poly(amido-amines)s by size exclusion chromatography. Biomed. Chromatogr. 19, 196–201.

Murthy, N., Robichaud, J., Tirrel, D., Stayton, P., Hoffman, A., 1999. The design and synthesis of polymers for eukaryotic membrane disruption. J. Contr. Release 61, 137–143.

Nakamura, K., Shikata, T., Takahashi, N., Kanaya, T., 2005. Highly extended conformation of polyelectrolytes incorporated into hybrid threadlike micelles studied by small angle neutron scattering. J. Am. Chem. Soc. 127, 4570–4571.

Nishida, K., Kaji, K., Kanaya, T., Shibano, T., 2002. Added salt effect on the intermolecular correlation in flexible polyelectrolyte solutions: small-angle scattering study. Macromolecules 35, 4084–4089.

Ohana, P., Gofrit, O., Ayesh, S., Al-Sharef, W., Mizrahi, A., Birman, T., Schneider, T., Matouk, I., de Groot, N., Tavdy, E., Sidi, A.A., Hochberg, A., 2004. Regulatory sequences of the H19 gene in DNA based therapy of bladder. Gene Ther. Mol. Biol. 8, 181–192.

Pack, D.W., Hoffman, A.S., Pun, S., Stayton, P., 2005. Design and development of polymers for gene delivery. Nat. Rev. Drug Discov. 4, 581–593.

Pattrick, N.G., Richardson, S.C.W., Casolaro, M., Ferruti, P., Duncan, R., 2001a. Poly(amidoamine) mediated intracytoplasmic delivery of ricin A-chain and gelonin. J. Contr. Release 77, 225–232.

Pattrick, N.G., Ferruti, P., Duncan, R., 2001b. Demonstration of poly(amidoamine)-mediated lysosomal membrane perturbation after administration to rats in vivo. Proc. Int. Symp. Contr. Release Bioact. Mater. 28, 864–865.

Pederson, J.S., 2002. Modelling of small-angle scattering data from colloids and polymers systems. In: Lindner, P., Zemb, Th. (Eds.), Neutrons, X-rays and Light: Scattering Methods Applied to Soft Condensed Matter. North-Holland.

Qin, L.H., Pahud, D.R., Ding, Y.Z., Beilinska, A.U., Kukowska-Latallo, J.F., Baker, J.R., Bromberg, J.S., 1998. Efficient transfer of genes into murine cardiac grafts by starburst polyamidoamine dendrimer. Hum. Gene Ther. 9, 553–560.

Ramzi, A., Scherrenberg, R., Joosten, J., Lemstra, P., Mortensen, K., 2000. Structure–property relations in dendritic polyelectrolyte solutions at different ionic strength. Macromolecules 35, 827–833.

Raper, S.E., Chirmule, N., Lee, F.S., Wivel, N.A., Bagg, A., Gao, G.P., Wilson, J.M., Batshaw, M.L., 2003. Fatal systemic inflammatory response syndrome in a ornithine transcarbamylase deficient patient following adenoviral gene transfer. Mol. Genet. Metab. 80, 148–158.

Richardson, S.C.W., Ferruti, P., Duncan, R., 1999. Poly(amidoamine)s as potential endosomolytic polymers: evaluation in vitro and body distribution in normal and tumour-bearing animals. J. Drug Target. 6, 391–404.

Richardson, S.C.W., Pattrick, N.G., Man, Y.K.S., Ferruti, P., Duncan, R., 2001. Poly(amidoamine)s as potential nonviral vectors: ability to form interpoly electrolyte complexes and to mediate transfection in vitro. Biomacromolecules 2, 1023–1028.

Sonawane, N.D., Szoka, F.C., Verkman, A.S., 2003. Chloride accumulation and swelling in endosomes enhances DNA transfer by polyamine–DNA polyplexes. J. Biol. Chem. 278, 44826–44831.

Wagner, E., 2004. Strategies to improve DNA polyplexes for in vivo gene transfer: will artificial viruses be the answer? Pharm. Res. 21, 8–14.

Wan, K.-W., Malgesini, B., Verpilio, I., Ferruti, P., Griffiths, P.C., Paul, A., Hann, A.C., Duncan, R., 2004. Poly(amidoamine) salt form affects pH-dependent membrane activity and polymer conformation in solution. Biomacromolecules 5, 1102–1109.

Wu, G.Y., Wu, C.H., 1988. Receptor-mediated gene delivery and expression in vivo. J. Biol. Chem. 262, 14621–14624.